Ultra-Thin Submillimeter Wave Absorbers for Bolometric Applications

Sergey A. Kuznetsov[1], Andrey G. Paulish[2], Alexander V. Gelfand[2],
Pavel A. Lazorskiy[2], Andrey V. Arzhannikov[1], and Victor N. Fedorinin[2]
[1]Novosibirsk State University & Budker Institute of Nuclear Physics SB RAS, Pirogova St. 2, Novosibirsk, 630090 Russia
2Institute of Semiconductor Physics SB RAS, Novosibirsk Branch "TDIAM", Lavrentiev Ave. 2/1, Novosibirsk, 630090 Russia

***Abstract*-The concept of electrically thin electromagnetic absorbers intended for applications in spectrally selective unclooled bolometric detectors and imaging systems operated in the range of submillimeter waves is discussed. The absorbers utilize a high impedance surface configuration and are implemented on basis of low-loss polymeric substrates and high conductivity metallization. A theoretical analysis is supplemented with experimental investigations of the high-performance ultra-thin absorbers with the wavelength-to-thickness ratio ~ 40-100 realized for the frequency band 200-400 GHz.**

I. Introduction

The rapid development of research in the range of submillimeter or terahertz waves of the electromagnetic spectrum demands adequate 2D matrix receivers for radiation detection, which are desired to be inexpensive, uncooled, easy-to-use, fast-response, sensitive, high-resolved, large-formatted, and capable of operating in real time. By now, implementation of THz matrix receivers maximally satisfied the aforementioned conditions faces serious instrumental restrictions arisen from specificity of the conventional approaches [1, 2]. The key drawback of commonly used THz sensors based on semiconductor and superconductor structures is connected with high complexity of their on-chip micro/nano-element integration & micro/nano-machining fabrication, unsuitable for large-format array mass production, or with the necessity of cryogenic environment. Similarly, the attempts for direct adaptation of modern room-temperature IR bolometric and pyroelectric array cameras, as well as fluorescence-quenching-based thermal image plates to THz imaging typically reveal either the problems of faint susceptibility or dimension restrictions for the radiation sensitive area, poorly applicable for handling radiation beams with diameters above 20 mm. Due to the aforementioned limitations, the high-quality THz imaging is typically realized via a time-consuming procedure of 2D raster scanning in a scheme with single detector measurements.

One of the prospective approaches to the real-time THz imaging is the uncooled bolometric detector based on a 2D array of micro-Golay (optoacoustic) cells and optical readout system, which was recently proposed by our group and realized in the far infrared region [3, 4]. The alternative scheme for bolometric detection of THz radiation can be built using the principle of terahertz-to-IR conversion [5]. Both the micro-Golay cell array detector and the THz-to-IR converter are estimated to be flexible to the choice of the operating wavelength and have no principle constraint on the array's overall dimensions. It is essential that adaptation of these detectors to the submm-wave band became feasible due to elaboration of the concept of electrically thin electromagnetic absorbers with a close to unity absorptivity within a desired frequency range [6-8]. Such absorbers are considered as a kind of metamaterial structures and can be effectively designed by using a concept of high-impedance (HISs) or artificial impedance surfaces (AISs) [6, 9]. Unlike the classical Salisbury, Jaumann, or Dallenbach electromagnetic absorbers based on unfavorably thick quarter-wave absorbing layers [10], the AIS-absorbers are capable of attaining the excess of at least several tens for the free-space wavelength λ ratio to the absorber thickness *d*. The condition $\lambda/d >> 1$ is essential for decreasing the absorber's heat capacity that allows achieving high sensitivity and low response time of the bolometric detector. It is noteworthy that the increase of the λ/d ratio inevitably leads to decreasing the absorption bandwidth, making AIS-absorbers ideally suitable for bolometric detectors with a high spectral resolution.

In this communication we present the results of the work on developing spectrally selective ultra-thin AIS-based absorbers designed for bolometric applications at frequencies ~ 200-400 GHz. The absorbers are implemented on basis of low-loss bulk materials, such as polypropylene dielectric films and high-conductivity aluminum metallization, that distinguishes them from any types of absorbers realized before. The paper is organized as follows: we start with illustrating the concepts of the micro-Golay cell array and the THz-to-IR converter with intergraded AIS-based absorbing layers. The theory basics for ultra-thin AIS-absorbers are presented afterwards and their fundamental features, analyzed via appealing an equivalent circuit model and 3D full-wave electromagnetic simulations, are discussed. In the rest of the paper we present the development results for narrow-band polarization-sensitive AIS-based absorbers with the λ/d ratio ~ 40-100, which high performance is demonstrated in "THz-to-IR conversion" experiments on imaging submm-wave beams from a backward wave oscillator of the milliwatt output radiation power level.

II. Concepts of Uncooled Bolometric Detectors

We develop two concepts of the uncooled bolometric detectors operated at room temperature and applicable to large-format multi-spectral THz imaging: the micro-Golay cell array

and the THz-to-IR converter. The detector schemes and operation principles are described below.

A. Micro-Golay Cell Array

In single-detector implementation, a Golay cell (GC) or optoacoustic cell is a well-known sort of radiation detectors exhibiting the highest sensitivity under room temperature operation [1, 2]. The GC is represented by an enclosed pneumatic gas chamber (Fig. 1 a), which front surface acts as an absorber for incoming radiation, while its opposite face is made as a flexible membrane with a mirror coating. The incoming radiation heats up the absorber, which transfers energy to the gas and induces its thermal expansion. The resulting pressure boost deforms the flexible membrane, leading to deflection of the optical beam from a light emitting diode that is further registered by a photodetector.

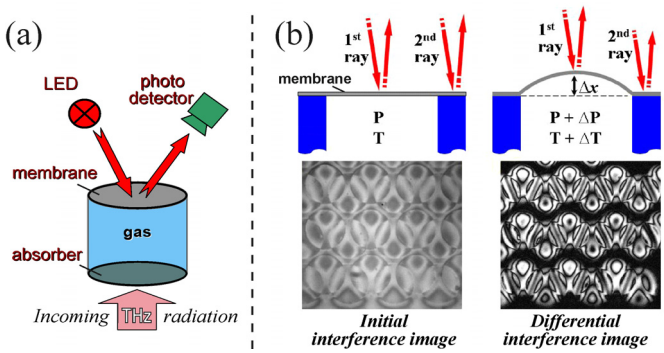

Figure 1. a) Operation principle of the Golay cell detector.
b) Illustration of the differential optical method for reading out the membrane deformation in the matrix structure of micro-Golay cells.

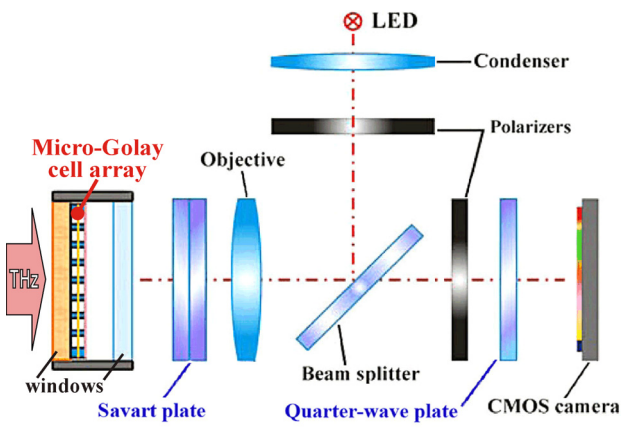

Figure 2. Schematic of the optical readout system for the micro-Golay cell array. The key element is the Savart plate, which splits the light radiation beam onto two co-directional orthogonally polarized but transversely shifted light beams. Reflected from the MGCA's membrane surface and passed through the quarter-wave-plate, these coherent beams become co-polarized and form the interference image in the focal plane of the CMOS camera.

The modern commercially available GCs demonstrate extremely broadband and almost flat spectral sensitivity ranging from the near infrared to millimeter waves. Along with high sensitivity values, this is realized due to a "black body absorptivity" scheme, when the incoming radiation is captured inside a sphere with high reflectivity walls and is eventually absorbed by an absorbing film placed inside the sphere. Such a scheme with multi-pass absorption inevitably leads to increasing the linear dimensions of the GC detector (typically up to 50-100 mm) that makes it inapplicable to realization of imaging array structures. In [3, 4] we avoided employing the reflecting spheres and implemented for the first time the large-format micro-Golay cell array (MGCA), which was designed for imaging applications at the long-wavelength infrared region (λ=8-14 μm). The developed MGCA is a planar structure, which was fabricated using lithographic techniques and included 200×200 operating cells with typical cell dimensions ∅100×50 μm.

It is noteworthy that our fabrication technology is flexible for rescaling MGCA to the terahertz band. It is also important that the real-time imaging with a large-format MGCA became feasible due to invention of an original differential optical method used for simultaneous detection of membrane deformation in all cells of the MGCA [11]. This method is based on registering the interference pattern between two coherent linearly polarized light beams propagating co-directionally but transversely shifted at the distance of a half-diameter of the optoacoustic cell (Fig. 1 b). The differential interference image appeared due to membrane deformation is resulted from the phase incursion for partial rays reflected from the movable central parts of the membranes. The proposed method enables to separate the detection & readout subsystems and to realize an effective scheme with registering the interference image by a conventional CMOS camera (Fig. 2). This approach removes fundamental limitations on the operating wavelength and the overall dimensions of the MGCA detector, as compared to other types of matrix THz sensors.

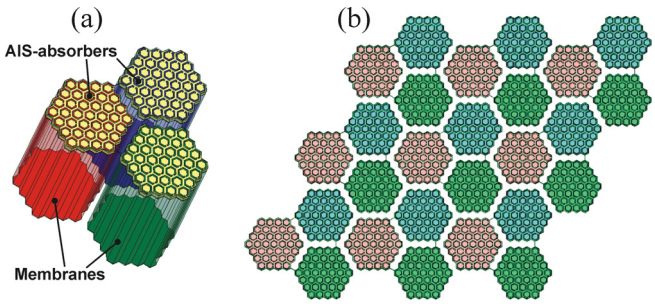

Figure 3. Concept of MGCA for three-spectral ("RGB-like") imaging at submm waves: a) triplet of elementary "pixels"; b) matrix structure of "pixels". Spectral discrimination is realized due to employment of the AIS-absorbers with spectrally shifted absorption bands (distinguished by colors).

Unlike the conventional single-detector GCs, the specifics of the proposed MGCA is in single-pass illumination of the micro-cell absorbers by incoming radiation. For the FIR MGCA we used SiO_2 layers as radiation absorbers, which single-pass absorptivity was limited by the value of several percent. By attracting the AIS concept to the absorber's design, close to 100% resonant absorptivity can be easily attained

under single-pass illumination condition, favorably combined with the "$\lambda / d >> 1$"-criterion. Fig. 3 illustrates an artistic view for a three-spectral ("RGB-like") MGCA, which matrix structure is formed by the triplets of optoacoustic cells with spectrally discriminated AIS-absorbers. Implementation of such a MGCA for the submm-wave band is in progress.

B. THz-to-IR Converter

The structure of the THz-to-IR converter and the proposed THz imaging system are shown in Fig. 4 and Fig. 5. The converter is represented by a multi-layer thin film structure, which includes an ultra-thin AIS used as the high-performance THz absorber and a thin layer with a perfect emissivity factor for IR radiation. Close to unity resonant absorption of the THz waves induces the converter heating that yields enhancement of IR emission from the emissive layer. The IR emission is detected by a commercial IR camera. In comparison with a micro-Golay cell array, a THz-to-IR converter is estimated to have the lower sensitivity to THz radiation but is much simpler in realization. Our experiments show that the proposed converter ideally suits for imaging submm-wave beams from backward wave oscillators with a milliwatt output radiation power level (see Section IV).

Similar to the MGCA absorbers, the converter's AIS is implemented as a three-layered structure and consists of a caring dielectric substrate (polypropylene, PP), a micropatterned subwavelength frequency selective surface (FSS) directed towards incident THz radiation, and a solid metallized layer ("GL") deposited on the opposite side of the PP substrate. By partitioning the converter surface onto sections, which differ in FSS geometries, the multi-spectral matrix structure can be realized.

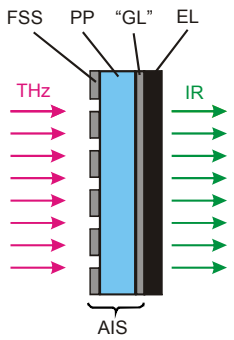

Figure 4. Structure of THz-to-IR converter. The frequency selective surface (FSS), polypropylene film (PP) and "ground" layer ("GL") form the artificial impedance surface (AIS), EL is an IR emissive layer.

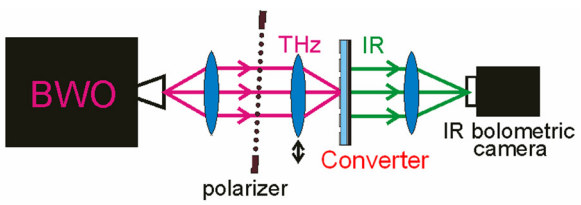

Figure 5. Scheme of THz imaging system based on THz-to-IR converter and IR bolometric camera. A backward wave oscillator (BWO) is shown as a THz source. The lens in front of the converter is optional.

III. Theory Basics for Ultra-thin Absorbers

The ideology of high-performance electromagnetic absorbers exhibiting a considerable excess of the operating free-space wavelength λ over the absorber thickness d is built on manipulating a spatial distribution of the electromagnetic filed and can be effectively formulated in terms of high-impedance or artificial impedance surfaces [6, 9].

When illuminated by a plane electromagnetic wave, the surface impedance Z, defined as the ratio of the tangential components of electric E and magnetic H fields upon the surface, specifies the amplitude reflectivity coefficient ρ according to the following formula:

$$\rho = \frac{Z - Z_0}{Z + Z_0}.$$

Here, Z_0 is the impedance of space, which borders on the surface and wherein the incident wave propagates ($Z_0 \cong 377\ \Omega$ for the case of free space). For the low-impedance surfaces ($|Z| << Z_0$), such as normal metals, $\rho \cong -1$ ($|\mathrm{Arg}(\rho)| \cong \pi$) due to vanishing the tangent component of the total electric field upon the surface, where the magnetic field doubles (Fig. 6 a). In this case the electric field antinode is formed at the quarter-wavelength distance from the surface, so the effective wave absorption can be achieved by introducing a lossy material into the field antinode, as it is realized in conventional absorbers of a "Salisbury screen" type. In general, such absorbers are estimated to be poorly attractive for bolometric applications since: a) realized on basis of quarter-wavelength solid substrates, they are seen as unfavorably "thick"; b) implemented with thin resistive sheets suspended at the $\lambda/4$-distance from the low-impedance surface, the absorber fabrication technology becomes too complicated and poorly compatible with MGCA and THz-to-IR converter concepts.

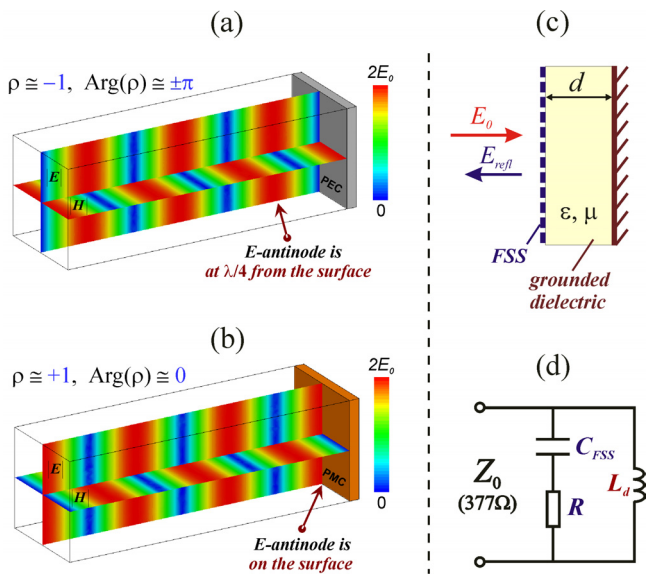

Figure 6. Simulated field distribution for marginal cases of impedance surfaces under plane wave illumination: a) Z=0 (perfect electric conductor); b) Z=∞ (perfect magnetic conductor). Schematic (c) and simplest equivalent circuit model (d) for AIS absorber utilizing high-impedance surface configuration.

By substituting the low-impedance surface for the high-impedance one ($|Z| >> Z_0$), which yields the amplitude reflectivity $\rho \cong +1$ and reflection phase $\mathrm{Arg}(\rho) \cong 0$, the electric field antinode can be shifted from the $\lambda/4$-distance outside the surface directly onto it (Fig. 6 b). It makes the high-impedance surfaces (HISs) ideally applicable to bolometers.

In a conventional design, the electrically thin HIS is realized as a subwavelength single-layer FSS of a capacitive kind placed over a thin "grounded" dielectric slab (Fig. 6 c). Under condition $d/\lambda << 1$, the impedance of the slab Z_d is purely inductive and proportional to its thickness d: $Z_d \cong j\omega L_d \cong j\,\omega Z_0 \mu\, d/c$, where ω is the radiation circular frequency, μ is the slab's relative permittivity ($\mu \approx 1$ at THz), and c is the light speed. If the inductive component of the FSS impedance Z_{FSS} is negligible in comparison with its capacitive part $1/j\omega C_{FSS}$ and dielectric or ohmic losses are absent (R=0), the HIS impedance is the impedance of the resonant circuit formed by connected in parallel L_d and C_{FSS} elements (Fig. 6 d):

$$Z = j\omega L_d/(1-\omega^2 L_d C_{FSS}).$$

Evidently, $Z \to \infty$ at the HIS resonant frequency $\omega_{HIS} = (L_d C_{FSS})^{-1/2}$ corresponding to maximization of the surface electric field under $d/\lambda << 1$ condition. The relative bandwidth $\Delta\omega_{HIS}/\omega_{HIS}$ of the HIS resonance, typically derived from the criterion $|\mathrm{Arg}[\rho(\omega_{HIS} \pm \tfrac{1}{2}\Delta\omega_{HIS})]| = \pi/2$ is evaluated as

$$\frac{\Delta\omega_{HIS}}{\omega_{HIS}} \cong \frac{1}{Z_0}\cdot\sqrt{\frac{L_d}{C_{FSS}}} \cong 2\pi\mu\cdot\frac{d}{\lambda}$$

that elucidates inevitability of the narrow-band operation when minimization of the structure's thickness is desired.

The ultra-thin absorber regime directly follows from the HIS regime when the dielectric or ohmic losses are properly incorporated into the dielectric slab or FSS metallization. This corresponds to introducing an effective resistor R connected in series to the lumped FSS capacitance C_{FSS} (Fig. 6 d). In the strict sense, the regime of perfect absorption differs from the HIS regime ($|Z| >> Z_0$) as it requires fulfilling the conditions

$$Re(Z) = Z_0,\ Im(Z) = 0. \qquad (1)$$

Due to this reason, the HIS-based absorbers are referred herein to as the artificial impedance surfaces (AISs) which satisfy the relations (1) at the AIS resonance.

By applying (1) to the equivalent circuit from Fig. 6 d, we can find that the optimal slab inductance L_d (and therefore the slab thickness d) resulting in total absorption is directly proportional to the resistance R:

$$L_d = C_{FSS} Z_0 R.$$

In case when $R << Z_0$, the absorption resonance is positioned at the frequency $\omega_{abs} \cong (L_d C_{FSS})^{-1/2} \cong (Z_0 R)^{-1/2}/C_{FSS}$ having the relative bandwidth at half maximum

$$\frac{\Delta\omega_{abs}}{\omega_{abs}} \cong 2\sqrt{\frac{R}{Z_0}} \cong 4\pi\mu\cdot\frac{d}{\lambda}. \qquad (2)$$

The relations (2), (3) clearly show that to minimize the thickness of the AIS-absorber, as well as to enhance its spectral selectivity, the dissipative parameter R should be minimized. It necessitates application of low-loss bulk materials in the absorber's configuration. Due to this reason, in this work we intentionally employed a polypropylene film as a caring dielectric substrate ($n \approx 1.5$, $\tan\delta \le 10^{-3}$) and high-conductivity metallization ($\sigma \approx 2\cdot 10^7$ S/m) utilized in the FSS and "ground" layers. Our analysis also shows that for all the investigated PP-based AIS the energy dissipation occurs mainly in the metallized FSS layer, unlike the results of other research groups reported on absorption predominance in the dielectric substrate [6-8].

Figs. 7 a-f illustrate phenomenology of ultra-thin AIS-absorbers by the example of AIS with a patch array FSS studied via a 3D full-wave electromagnetic analysis in the Ansoft HFSS™ software. The 2D patch array was chosen to

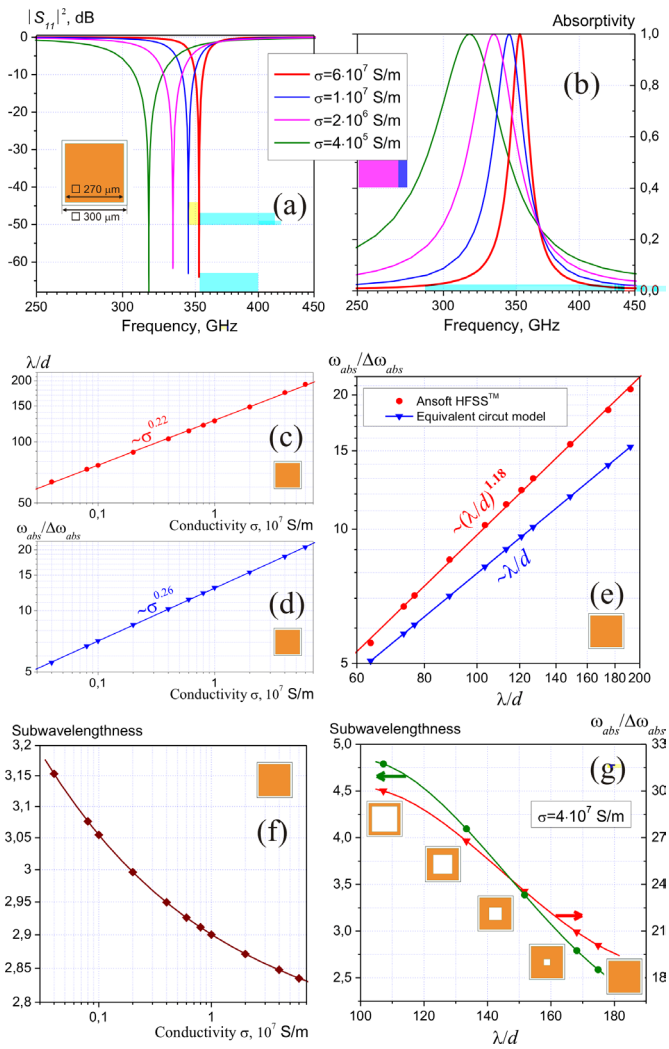

Figure 7. Simulated characteristics of submm-wave AIS-absorbers with a patch array FSS at optimized slab thickness: a, b) spectral behavior of reflection and absorption coefficients at different values of electrical conductivity of patches; c, d, f) wavelength-to-thickness ratio, absorptivity Q-factor and FSS subwavelengthness as the functions of conductivity; e) Q-factor versus wavelength-to-thickness ratio. f) Improvement of FSS subwavelengthness and AIS spectral selectivity via topology modification: "patch→ ring".

have a square symmetry at the lattice constant g=300 μm and inter-patch separation 30 μm. Figs. 7 c, d show that the absorber's wavelength-to-thickness ratio λ / d and the Q-factor $\omega_{abs}/\Delta\omega_{abs}$ are proportional approximately to the forth root of the electric conductivity σ, ranging from 64 to 192 and from 6 to 21 respectively when σ increases from $4{\cdot}10^5$ S/m to $6{\cdot}10^7$ S/m. The dependence $\omega_{abs}/\Delta\omega_{abs}(\lambda/d)$ exhibits some deviation from the linear law (2) that is associated with an unaccounted inductive term in the FSS impedance upon its interaction with the ground plane. We also note that the FSS subwavelengthess factor S, defined as the ratio of the resonant absorption wavelength λ to the FSS lattice constant g, decreases when σ grows (Fig. 7 f.). Such a behavior follows from the equivalent circuit model, which states that $\lambda \propto R^{-1/2}$. For the AIS with a patch array FSS $S \sim 3$ that is seen to be insufficiently small when the pixel dimensions of the imaging bolometric detector are desired to be minimized. AIS subwavelengthness and spectral selectivity can be improved by employing a selfresonant FSS (e.g. a ring array FSS, Fig. 7 g), though in this case the AIS exhibits the lower λ / d ratios.

IV. Experimental Results

For implementing a submm-wave bolometric detector operated in the regime of spectral and polarization discrimination, we developed three different narrow-band polarization-sensitive AIS-absorbers designed for the fundamental absorption at the frequencies 0.30, 0.33, and 0.36 THz respectively. A polypropylene film with thickness d=20 μm was used as the AIS dielectric substrate, further metallized from both sides via a thermal vacuum deposition of aluminum 0.4 μm thick to form the high-conductivity metallization of the "ground" and FSS layers. The photolithographically-patterned split ring resonator arrays (SRRs) were utilized in the AIS configurations as the polarization-selective FSSs (Fig. 8). The choice of SRR topology allowed use to realize the values of the subwavelengthness factor $S \sim$ 8-9.

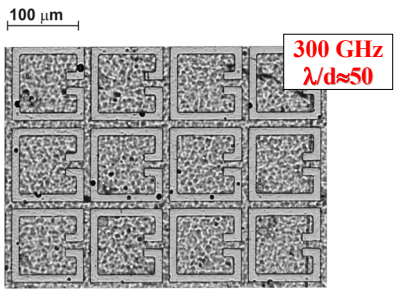

Figure. 8. Micrograph of topological pattern for SRR FSS fabricated on PP surface (example of the 300 GHz absorber with $\lambda / d \approx 50$). The manifested irregularities are associated with granularity and roughness of the PP film.

All the absorbers were numerically optimized in Ansoft HFSS™ by exploiting the regime of Floquet ports and periodic boundary conditions applied to the AIS unit cell. For the fixed PP thickness the optimal combination of SRR geometry parameters, providing the reflectivity factor $|S_{11}|^2$ below -30 dB at the fundamental resonance frequency ν_{abs} of the each absorber (0.30, 0.33, and 0.36 THz), were numerically determined to realize the ratios $\lambda / d = 50, 45,$ and 41 respectively. The spectral behaviour of the absorption coefficient $A = 1 - |S_{11}|^2$, derived from the simulated and experimentally measured reflectivity related to the normal excitation, is shown in Fig. 9. The left and right spectra correspond to co-polar (E ⊥ SRR gaps) and cross-polar (E || SRR gaps) polarization modes respectively. The rather good agreement between simulations and measurements can be seen from the figure. The relative bandwidth $\Delta\nu_{abs}/\nu_{abs}$ of the co-polar absorption resonance is estimated as 6% for experimental data versus 4.5% for the simulated one. A discrepancy between simulations and measurements is attributed to deviations of the material parameters from the nominal values used in simulations.

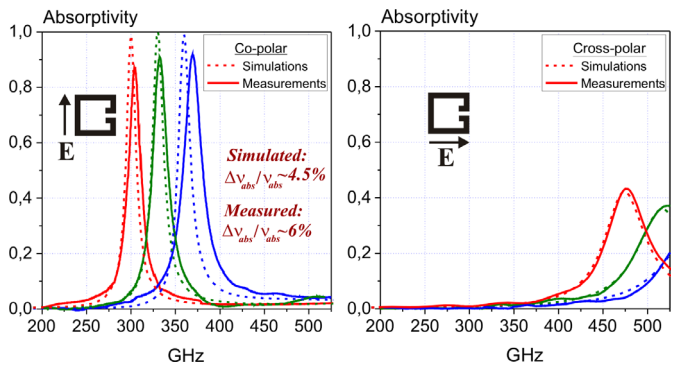

Figure 9. Spectral response of three different SRR-based ultra-thin AIS-absorbers for mutually orthogonal polarizations.

The developed AIS-absorbers were used in the design of the proposed THz-to-IR converter shown in Fig. 4. As the IR emissive layer, we employed a graphitized coating 10 μm thick deposited over the outer surface of the "ground" AIS layer. The experimentally measured IR emissivity factor was around 93%.

By using the THz-to-IR converter, the THz imaging system shown in Fig. 5 has been realized in this work. The backward wave oscillator (BWO) with tuneable output wavelength and 3-10 mW emission power was employed as the source of monochromatic terahertz radiation both for imaging experiments and AIS characterization. The example of the image for the unfocused BWO beam, obtained for the converter with the resonant frequency 0.3 THz at co-polar excitation, is shown in Fig. 10. We have employed the converter with a clear aperture diameter 32 mm. The beam half-width, estimated from the IR image, was around 16 mm. It is noteworthy that the IR signal disappears for THz frequencies out of the absorber's sensitivity band.

The high polarization sensitivity of the converter has been demonstrated via converter rotation relative to the polarization vector of the incident beam (Fig. 11). The beam focusing was used to increase the dynamic range of measurements. The transition from the co-polar (Fig. 11 a) to cross-polar (Fig. 11 b) excitation regime results in a signal decrease down to a zero level.

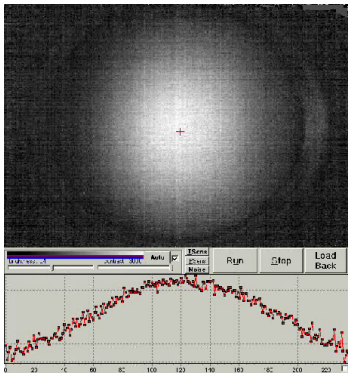

Figure. 10. IR Image of the unfocused co-polarized BWO beam for the converter with resonant frequency 0.3 THz. The bottom graph indicates intensity distribution along the horizontal line traced through the red crosshair.

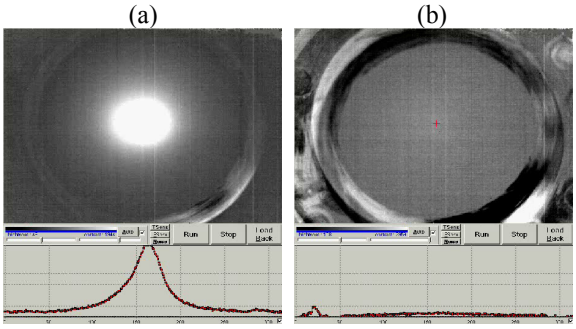

Figure 11. Images of the unfocused BWO beam for different polarizations: a) E ⊥ SRR gaps; b) E || SRR gaps. Example of 0.3 THz-absorber.

The possibility of the real-time THz imaging has been shown in a series of experiments including visualization of manually controlled free motions of the focused submm-wave beam along the converter surface (Fig. 12). We also revealed the negative effects of the "comet tail" and blooming. One of the ways for their reducing is to thin further the converter. This can be achieved via employing the AIS with a thinner dielectric substrate and an appropriately redesigned FSS pattern. Fig. 13 illustrates our first result on implementation of the AIS-absorber with λ / d - ratio ≈ 100 optimized for near-unity co-polar absorption at 200 GHz. The gangbuster FSS and PP film 15 μm thick were utilized in the absorber configuration.

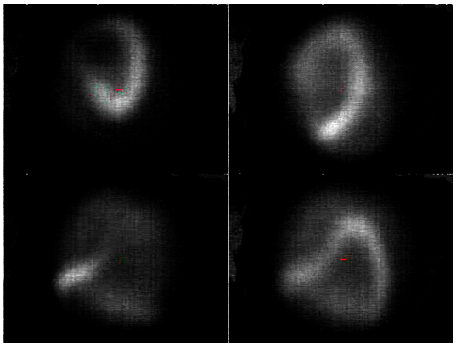

Figure. 12. Screen shots from the recorded movie at real-time THz imaging: motions of the focused submm-wave beam along the converter surface.

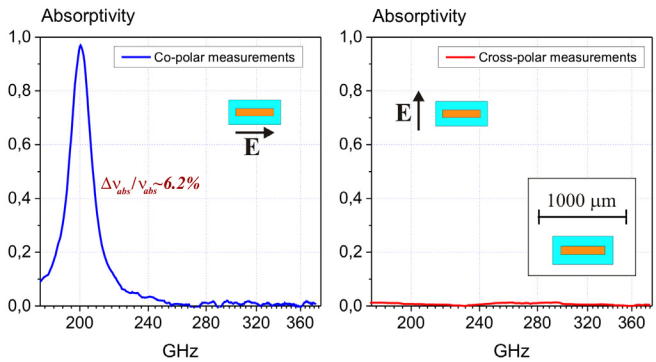

Figure 13. Measured spectral absorptivity for the ultra-thin AIS-absorber with wavelength-to-thickness ratio $\lambda / d = 100$ optimized for near-unity co-polar absorption at 200 GHz. The gangbuster FSS unit cell is shown in the inset.

V. Conclusions

In this contribution we introduced the concepts of the micro-Golay cell array and the THz-to-IR converter, as the uncooled bolometric detectors flexible both for single-pixel and large-format imaging array implementation at submm waves. As the spectrally selective radiation-sensitive elements for such detectors, the high-performance ultra-thin absorbers utilizing the ideology of artificial impedance surfaces are proposed. The theory basics for AIS-absorbers are considered and preference of using the low-loss bulk materials, such as polypropylene films and high-conductivity aluminium-like metallization, in absorber's configurations is highlighted. The experimental testing of the AIS-absorbers developed for the frequency range 200-400 GHz and exhibiting wavelength-to-thickness ratios ~ 40-100 confirms effectiveness of the proposed approach.

Acknowledgments

This work is supported by the grant 11.G34.31.0033 of the Russian Federation Government and the contract 16.740.11.0377 via the Federal Target Program.

References

[1] L.Yun-Shik, *Principles of THz Science and Technology,* Springer, 2009.
[2] F. Sizov, "THz radiation sensors," *Opto-Electron. Rev.*, vol. 18, no. 1, pp. 10-36, 2010.
[3] A. V. Gelfand et al., "Uncooled matrix IR detector based on optoacoustic cells and optoelectronic reading system," *Opt. Memory & Neural Networks*, vol. 18, no. 1, pp. 25-28, 2009.
[4] S. A. Kuznetsov et al., "Implementation of Novel Type of IR-THz Receivers Based on Matrix Structures of Optoacoustic Cells", *Proc. of the 40th European Microw. Conf.* (EuMC-2010), pp. 61-64, 2010.
[5] S. A. Kuznetsov et al., "Bolometric THz-to-IR converter for terahertz imaging," *Appl. Phys. Lett.,* in press.
[6] O. Luukkonen et al., "A thin electromagnetic absorber for wide incidence angles and both polarizations," *IEEE Trans. on Antennas and Propagation*, vol. 57, n. 10, pp. 3119-3125, 2009.
[7] H. Tao et al., "Highly flexible wide angle of incidence terahertz metamaterial absorber: Design, fabrication, and characterization," *Phys. Rev. B*, vol. 78, Iss. 24, pp. 241103-1-4, 2008.
[8] X. Liu et al., "Infrared Spatial and Frequency Selective Metamaterial with Near-Unity Absorbance," *Phys. Rev. Lett.,* vol. 104, pp. 207403-1-4, 2010.
[9] C. A. Balanis, *Modern Antenna Handbook*, Wiley-Interscience 2008.
[10] K. J. Vinoy, R, M, Jha, *Radar absorbing materials: from theory to design and characterization*, Kluwer Academic Publishers 1996.
[11] V.N. Fedorinin, Russian Federation Patent 2 157 513, 1999.